

## The potential of different Autotaxin inhibitor types regulating catalysis-dependent and -independent signalling

Fernando Salgado-Polo<sup>1</sup>, Anastassis Perrakis<sup>1\*</sup>

<sup>1</sup> Oncode Institute and Division of Biochemistry, Netherlands Cancer Institute, Plesmanlaan 121. 1066 CX, Amsterdam, the Netherlands.

\* Corresponding author.

### Abstract

Autotaxin (ATX) is a secreted lysophospholipase D, catalysing the conversion of lysophosphatidylcholine (LPC) to bioactive lysophosphatidic acid (LPA). LPA acts through two families of G protein-coupled receptors (GPCRs) controlling key cellular responses, and is implicated in many physiological processes and pathologies. ATX has therefore been established as an important drug target in the pharmaceutical industry. Structural and biochemical studies of ATX have shown that it has a bimetallic nucleophilic catalytic site, a substrate-binding (orthosteric) hydrophobic pocket that accommodates the lipid alkyl chain, and an allosteric tunnel that can accommodate various steroids and LPA. Here we first review what is known about ATX-mediated catalysis, crucially in light of allosteric regulation. We then present the known ATX catalysis-independent functions, including binding to cell-surface integrins and proteoglycans. In light of these data we then discuss the four types of ATX inhibitors, as classified depending on their binding to the orthosteric and/or the allosteric site. Finally, we analyse the binding mode of known members of all four types and discuss how mechanistic differences might differentially modulate the activity of the ATX-LPA signalling axis, and clinical applications including cancer.

### Keywords:

Lysophosphatidic acid, Autotaxin, inhibitor, allosteric, orthosteric, lipid chaperone, signalling, GPCR

## Introduction

Lysophosphatidic acid (1- or 2-acyl-*sn*-glycero-3-phosphate or LPA) is a bioactive lipid found in many body fluids and involved in many physiological and pathological processes. Historically, LPA was identified as a growth factor in serum that could induce motility in fibroblasts and cancer cells through GPCRs [1,2]. Subsequent research identified specific LPA GPCRs (LPA<sub>1-6</sub>), which have distinct expression patterns [3]. Deregulation of the LPA signalling axis has been linked to different diseases, such liver disease [4], fibrosis [5], pruritus [6], and cancer [7,8].

The LPA receptors are classified into distinct families, the EDG (LPA<sub>1-3</sub>) and non-EDG (LPA<sub>4-6</sub>) families. The crystallographic structures of LPA<sub>1</sub> and LPA<sub>6</sub> have provided the field with key mechanistic indications with respect to their ligand binding mode [9,10]. The LPA<sub>1</sub> substrate-binding site is located inside a central globular cavity capped by an extracellular N-terminal helical lid. The large (also named “baggy”) ligand-binding pocket remains closed at the membrane side, indicating it is solely accessible from the extracellular space. This enables LPA binding, but potentially phosphorylated endocannabinoids to bind and activate LPA<sub>1</sub>. Such an extracellular lipid-binding site capped by flexible helices is consistent with a model by which LPA is carried by a lipid chaperone, such as albumin, to bind to the flexible N-terminal domain of LPA<sub>1</sub> and deliver LPA specifically [9]. Conversely, the zebrafish LPA<sub>6</sub> structure [10] showed a much smaller ligand-binding site, that is not open towards the extracellular milieu, restricting the receptor’s specificity solely to LPA [10]. The LPA<sub>6</sub> structure is consistent with a binding mode by lateral diffusion of the LPA in the plasma membrane, which would not require lipid-carrying molecules to take place [11,12].

Since LPA can promote a plethora of downstream signalling events, both its production and degradation are tightly regulated, resulting in an estimated half-life of ~3 min in circulation [13–15]. Such a short-lived existence is due to its fast degradation by three membrane-bound lipid phosphate phosphatases (LPPs), which cleave the LPA phosphate group and release signalling-inactive monoacylglycerol [16,17]. Contrary to this, LPA production originates from two sources: phosphatidic acid hydrolysis by PLA<sub>1/2</sub> and from the enzymatic conversion of lysophosphatidylcholine (1- or 2-acyl-*sn*-glycero-3-phosphocholine or LPC) to LPA by a lysophospholipase D (lysoPLD) that has been established to be Autotaxin (ATX) (Figure 1) [18,19]. ATX-catalysed production constitutes the main physiological source of extracellular LPA, and therefore ATX has been widely studied as a target for drug development [13,20,21].

ATX is the only member of the Ectonucleotide Pyrophosphatase / Phosphodiesterase family (ENPP) that presents lysoPLD activity (*EC* 3.1.4.39) over lysophospholipids [21]. ATX is first translated as a pre-proenzyme that undergoes two proteolytic processing steps, resulting in a mature, glycosylated and secreted form [22]. The determination of the structure of ATX by X-ray crystallography enabled the determination of its domain organization: the two N-terminal somatomedin B (SMB)-like domains are followed by a central catalytic phosphodiesterase (PDE) domain, which is adjacent to an inactive nuclease-like domain. Substrate hydrolysis requires a bimetallic active site containing two Zn<sup>2+</sup> ions and a threonine nucleophile, which act in an associative two-step in-line displacement catalytic mechanism [23].

Structural studies have also established that ATX has a unique tripartite binding site. The catalytic bimetallic site is next to a hydrophilic shallow groove that accommodates the hydrophilic glycerol moiety of lipid substrates. This groove is connected by a T-junction to a hydrophobic pocket where acyl chains can bind, and a tunnel (often called the “hydrophobic channel”) that leads to the other side of the PDE domain [24]. It is noteworthy that the tunnel (or channel) is only partially hydrophobic in nature and has hydrophilic patches, unlike the pocket (Figure 2). The tunnel binds steroid molecules [25], as well as the LPA product [26,27], which results in a modulation of catalytic efficiency. Thus, we refer to the tunnel as the allosteric site, while we refer to the substrate-binding, hydrophilic groove and the hydrophobic pocket, as the orthosteric site (Figure 3).

Here, we will first review the catalytic mechanism of ATX, especially in light of the allosteric modulation we have recently described, discuss the non-catalytic functions of ATX, and how these are involved in the ATX-LPA signalling axis. Then, we will present the four families of ATX inhibitors from a structural biology perspective, as they are classified depending on their occupancy of the orthosteric and/or the allosteric site. Finally, we will discuss how the different types of inhibitors might interfere with catalytic and non-catalytic functions to differentially affect the ATX-LPA signalling axis *in vivo*.

## Autotaxin Catalytic and Non-Catalytic Functions

ATX has long been established as the lysoPLD that converts LPC into LPA, but the exact catalytic mechanism remained a subject of study and debate. The first complete characterization of ATX catalysis showed that LPC binding was slow and rate-limiting, and offered clear evidence for a model where catalysis first results in choline release, which is followed by the slow release of NBD-LPA (tens of seconds) [28]. More recently, we have observed a ~10-minute lag phase in time-course measurements of ATX activity, which could be alleviated by the addition of external LPA [27]. We proceeded to show that LPA binding increases the turnover rate ( $k_{cat}$ ) of LPC hydrolysis and promotes its own production. Specifically, our results established that binding of LPA takes place at the low-affinity (~1  $\mu$ M) tunnel allosteric site. This binding is consistent with earlier results [26] that attributed residual electron density in crystallographic structures of mouse Autotaxin to LPA (16:0, 18:0, 18:1, 18:3 and 22:6). However, molecular dynamics simulations and kinetic modelling [27] argue that the presence of LPA in the ATX allosteric tunnel is an independent event, which does not represent an exit pathway of produced LPA by LPC hydrolysis in the adjacent orthosteric site. Moreover, even though the tunnel does not play a critical role in recruiting LPC substrates from BSA or detergent micelles [26], introduction of different tunnel-occluding loop insertions, based on those present in ENPP1 and ENPP3, resulted in mutants with much impaired cell motility-stimulating activity. Although these observations appear contradictory, the loop insertions could have induced structural changes destabilising the orthosteric site, and resulting in catalytically inactive ATX without just occluding substrate trafficking through the tunnel. Interestingly, a recent study indicated that active ATX can bind to the surface of secreted exosomes and carry LPA [29]. Such an event could hypothetically lead to LPA-bound ATX at the cell surface, after which ATX would release LPA and activate LPARs. Indeed, the authors indicated that it was by this mechanism that ATX yielded activation of LPA<sub>1</sub> and LPA<sub>3</sub> in the employed *in vitro* experimental setup [29]. Taken together, the evidence is consistent with a role of ATX as an LPA carrier, transporting LPA to distal locations from those where LPC can be taken. LPC is present in the blood at high concentrations (100-200  $\mu$ M [18]); most of it is bound to serum albumin and cannot be “extracted” by ATX, while a small fraction (about 1  $\mu$ M) is free and can be recognized by ATX. The source of the LPC substrate poses another exciting question: its rate of production, lifetime in circulation, and local concentrations in specific organs have received rather limited attention compared to the importance of the question.

Besides its catalysis-dependent functions related to LPA production, ATX also mediates diverse cell signalling events through binding to integrins and heparan sulfate proteoglycans (HSPGs). On one hand, the more abundant ATX $\beta$  isoform binds to integrins, which in turn promotes cell proliferation [30] and directional cell motility [31]. This interaction takes place through the ATX SMB domains, which have high structural similarity with the SMB domain of the cell adhesion factor vitronectin. Specifically, ATX $\beta$  can interact with  $\alpha$ v $\beta$ 3 or  $\alpha$ IIb $\beta$ 3 integrins, both of which cause platelet activation upon interaction with ATX [24,32,33]. Accordingly, integrin binding enables uptake and intracellular sequestration of ATX, which redistributes to the front of the migrating cells. However, blockade of integrin binding did not abolish cell migration

completely. Interestingly, cell stimulation with only the ATX SMB domains promotes directional cell migration independently of lysoPLD activity [31]. On the other hand, the less abundant ATX $\alpha$  isoform (but not ATX $\beta$ ) binds to HSPGs through a polybasic insertion [34]. This interaction results in an increase of ATX $\alpha$  catalytic turnover, which may elicit a membrane-anchored burst of LPA production and downstream signalling. Even though this isoform-specific function lacks further characterization, it has been recently reported that ATX $\beta$  interacts in an SMB-independent manner with the HSPG syndecan-4, which affects cell proliferation and cellular metastatic potential [30]. Thus, accumulating evidence suggests several mechanisms for cell receptor binding in the ATX structure, highlighting the relevance of plasma membrane recruitment.

## The Autotaxin Inhibitor Family

Initially, classical ATX inhibitors relied on lipid analogues targeting ATX based on similarities with sphingosine-1-phosphate (S1P) or LPA. Activity-based lead discovery campaigns, using artificial substrates as activity reporters, subsequently made important contributions, many of which are reviewed in e.g. [35,36]. The structural characterization of rat and mouse ATX structures in 2011 [24,26], enabled a remarkable potential for selective inhibitor design by focusing on the three dimensional architecture of the ATX active site. While attention initially focused on the lipid-binding pocket and the catalytic site, current emphasis is on the so-called tripartite site that we introduced earlier (Figure 3).

The tripartite ATX binding site represents a remarkable potential for selective design of inhibitors. Over time, ATX inhibitors of distinct chemical nature were designed, including lipid-based inhibitors [37], DNA aptamers [38], as well as small molecules. The latter, the focus of this review, can be in turn classified in four distinct types (I, II, III, and IV) depending on their mode of binding to the ATX tripartite site (Figure 4) [39].

In this review we focus to compounds for which there is a crystal structure available, and we discuss their properties in light of their experimentally determined binding pose; in that sense the list of discussed compounds is not exhaustive but focused. It should be noted that, due to the unclear naming of some inhibitors as “Compound #” in the literature, we will refer to those as “FL-Cpd-#”, where FL stands for the first and last names of the publication’s first author.

### Type I Inhibitors

Type I compounds occupy the orthosteric site, mimicking the LPC substrate mode of binding. As such, they include competitive inhibitors with a long and flexible structure that occupies the catalytic site, the shallow groove and the hydrophobic pocket. Several analogues based on LPA have naturally been put forward as ATX inhibitors: cyclic phosphatidic acid or cPA ( $IC_{50} = 0.14 \mu\text{M}$ , bis-*p*NPP) [40], thiophosphate ( $IC_{50} = 0.6 \mu\text{M}$ , bis-*p*NPP) [41],  $\alpha$ -bromomethylene phosphonates like BrP-LPA ( $IC_{50} = 0.7\text{-}1.6 \mu\text{M}$ , LPC) [42], the synthetic analogue for S1P FTY720-P ( $K_i = 0.2 \mu\text{M}$ , Bis-*p*NPP) [43], and the most potent lipid-based inhibitor S32826 ( $IC_{50} = 5.6 \text{ nM}$ , LPC) [44]. The latter showed poor *in vivo* stability, which prevented it from further use in animal models.

The first small molecule type I inhibitors were thiazolidinediones discovered in a screen using the artificial substrate CPF4 [13,24]. Optimisation led to the identification of HA-130 ( $IC_{50}$  = 28 nM, LPC), a boronic acid-based inhibitor that could attack the nucleophilic oxygen at the catalytic threonine and it was able to hamper LPA production both *in vivo* and *in vitro* [13]. Moreover, a positional isomer of HA-130, HA-155 ( $IC_{50}$  = 5.7 nM, LPC) (Figure 5) was co-crystallized with ATX, which revealed interactions with Thr209, Asp311, His359 and His474 at the active site, as well as Leu213, Phe274 in the hydrophobic pocket (Figure 3, Table 1). Based on HA-155 crystal structure, this series was subjected to structure-activity improvement studies. These consisted in trial of the different linkers added to the thiazolidine-2,4-dione core [45].

Subsequently, numerous type I ATX small molecule inhibitors have appeared in both academic and patent literature. An example of these are the thiazolone derivatives similar to the HA series produced by Kawaguchi and collaborators [46]. A library of 81,600 compounds was screened for inhibiting the hydrolysis of the fluorescence probe TG-mTMP. This led to the identification of KM-Cpd 10 (180 nM, TG-mTMP), 2BoA (580 nM, TG-mTMP), 3Boa (13 nM, TG-mTMP) and 4BoA (22 nM, TG-mTMP), which were co-crystallized with ATX (Figure 5). These structures revealed interactions with Arg284, as well as hydrophobic contacts with Trp260 and Phe274 (Figure 3, Table 1). Moreover, these compounds were able to decrease LPA levels both *in vitro* and *in vivo* [46].

The most potent type I inhibitor to date is PF-8380 ( $IC_{50}$  = 1.7 nM, LPC) (Figure 5), reported by Pfizer [47,48]. In general, it has been widely used because of its high potency and its favourable pharmacokinetic properties, which has allowed *in vivo* evaluation of ATX inhibition. PF-8380 is a benzoxazolone that exhibits the general chemotype of lipophilic tail, core spacer, and acidic head group. This general motif contains a benzoxazolone as the acidic head group, a functionalized piperazine as the spacer, and the dichlorocarbamate moiety as the lipophilic portion [47,48]. In the active site, the acidic head group makes essential interactions with one of the  $Zn^{2+}$  ions, and the lipophilic tail is accommodated within the hydrophobic pocket. Moreover, it is in close proximity to Thr209 and has hydrophobic interactions with Leu213, Phe273, Phe274, as well as a Hydrogen bond with the Trp275 amino group (Figure 3). The addition of a hydroxyethyl group to PF-8380 resulted in FP-Cpd-3, which had an increased solubility and was co-crystallisation with ATX (Figure 5) [49]. ATX inhibition with PF-8380 was shown to attenuate bleomycin-induced pulmonary fibrosis, owing to decreased LPA levels in plasma and bronchioalveolar lavage fluid, together with a decrease in inflammation and collagen deposition (Table 2). However, effectiveness of treatment with this compound varies in the literature [50,51]. Recently, treatment of mice in a high fat-diet with PF-8380 reduced plasma LPA levels, resulting in lower diet-induced cardiac dysfunction and inflammatory response [52].

The compound SBJ-Cpd-1 ( $IC_{50}$  = 520 nM, LPC) [47] (Figure 5) was obtained from an aminopyrimidine series that was further improved by addition of the benzoxazolone moiety present in PF-8380. This was crucial for synthesizing the far more active SBJ-Cpd-2 ( $IC_{50}$  = 2.5 nM, LPC), which reaches the active site  $Zn^{2+}$  ions in a similar manner to that of PF-8380. Additionally, it also contacts Asp171, Asp311, His315 and His474 at the active site, and Leu213, Phe273, Phe274

and Trp275 at the pocket (Figure 3, Table 1). This compound was further tested in rats by a single oral dose (10 mg kg<sup>-1</sup>), where plasma LPA levels decreased 80% upon 12-h treatment (Table 2). Lastly, another relevant compound shown to behave type I inhibitors is the benzotriazole BI-2545 (2.2 nM, LPC) [53] (Figure 5), which was able to reduce LPA levels both *in vitro* and *in vivo*.

### Type II Inhibitors

Type II ATX inhibitors owe their effect solely to binding to the hydrophobic pocket, where they obstruct LPC accommodation. As a result, this competitive mode of binding avoids interaction with the catalytic Zinc ions, which may offer selectivity advantages over other inhibitors. The artificial ATX substrate FS-3 was used by PharmAkaea to screen small molecule compounds, from which they identified four Indole-based analogues with high inhibitory potency. Among these, three lead type II compounds were reported, namely PAT-078 (IC<sub>50</sub> = 472 nM; LPC), PAT-494 (IC<sub>50</sub> = 20 nM; LPC) and PAT-352 (IC<sub>50</sub> = 26 nM; LPC) [54] (Figure 6). The structures of these compounds revealed common hydrophobic interactions between their vinyl-nitrile or hydantoin moieties, and Leu213, Leu216, Phe274, Trp275 and Tyr306 (Figure 3, Table 1).

The artificial ATX substrate FS-3 was also used as readout for a high-throughput screen from a collection of 87,865 compounds. Upon a preliminary selection of 1.2% best hits, the physiological LPC choline release assay was used, from which the imidazo[4,5-b]pyridine-derivative CRT0273750 (IC<sub>50</sub> = 1 nM, LPC; 14 nM human plasma LPC) [55] was identified (Figure 6). The crystal structure of ATX in complex with CRT0273750 indicated that the compound binds at the hydrophobic pocket, as well as with the boundaries of the ATX tunnel, but 5 Å away from the active site. As a consequence, it establishes a hydrogen bond with Lys247, and hydrophobic interactions with Leu213, Phe248, Trp254, Phe273, Phe274 and Trp275 (Table 1). *In vitro* data showed that this compound could inhibit migration of 4T1 cells. Moreover, the compound was effective in reducing 18:1 LPA levels *in vitro* in human plasma, as well as in *in vivo* samples from MDA-MB-231-*luc* tumor bearing Balb-c *nu/nu* mice (Table 2) [55]. Lastly, the short phosphonate lipid analogue GWJ-A-23 [56] can be found in Figure 6.

### Type III Inhibitors

Type III inhibitors specifically occupy the allosteric regulatory tunnel, modulating ATX activity by non-competitive inhibition. We have reported that 7- $\alpha$ -hydroxycholesterol (Figure 7) is commonly present in purified mammalian ATX structures, but this does not have an observable inhibitory activity. However, other steroids, and namely bile salts such as tauroursodeoxycholic acid (TUDCA) (IC<sub>50</sub> = 10.4  $\mu$ M; LPC) or ursodeoxycholic acid (UDCA) (IC<sub>50</sub> = 8.8  $\mu$ M; LPC) exert modest and partial (always leaving residual activity) non-competitive inhibition of lysoPLD activity (Figure7) [25]. The ATX co-crystal with 18:1 LPA bound at the orthosteric site and TUDCA bound at the tunnel confirmed the non-competitive mode of inhibition. TUDCA interacts with ATX, forming a hydrogen bond with Trp260 and hydrophobic stacking with Trp254 and Phe274 (Figure 3). The mechanism underlying its inhibition may occur by counteracting the modulatory action of LPA in the tunnel [27].

The identification of type II indole-based ATX inhibitors that we discussed above, also yielded a type III compound, namely PAT-347 ( $IC_{50} = 0.3$  nM; LPC) (Figure 7) [54]. The crystal structure of ATX bound to both PAT-347 and 14:0 LPA confirmed its non-competitive binding mode. PAT-347 accommodates at the tunnel by  $\pi$ - $\pi$  interactions between its indole moiety and Phe274 and His251. Moreover, its benzoic acid makes another  $\pi$ - $\pi$  interaction with Phe249. It also contacts with Lys248, Trp254 and Trp260. More recently, the pharmacokinetic properties of two novel compounds, PAT-505 ( $IC_{50} = 2$  nM; LPC) and PAT-048 ( $IC_{50} = 1.1$  nM; LPC) were assessed (Figure 7) [57–60]. The crystal structure of PAT-505 bound to ATX showed a very similar binding mode to that of PAT-347, namely by interacting with Lys248, Phe249, His251, Trp254, Trp260, Phe274, but also Ser81 and Val277 (Table 1). Clinical assays with PAT-048, showed better pharmacodynamics results, and this was used for *in vivo* assays with a bleomycin-induced mouse model for dermal fibrosis. Pharmacological inhibition of ATX activity markedly attenuated skin fibrosis upon treatment with  $10$  mg  $kg^{-1}$  PAT-048, which related to a 75% inhibition of ATX activity after 24h and >90% at double dose (Table 2). It is worthy to mention that five new patented PharmAkea compounds, namely PharmAkea-Cpd A-E ( $IC_{50} = <0.5$   $\mu$ M; LPC) have been recently used in metabolic disorder treatment, where they showed a decrease of fasting blood glucose levels in mice fed with a high-fat diet (Table 2) [61].

Another series of indole-derived type III compounds has been recently reported, resulting from a structure-activity evolution of a compound reported by Amira Pharmaceuticals [62], which led to the identification of LM-Cpd 51 [63] (Figure 7). The co-crystal structure with rat ATX showed that the compound binds in the tunnel, establishing stacking interactions with Trp254, as well as hydrophobic interactions with Phe249, Trp260 and Phe274 (Table 1).

### Type IV Inhibitors

Type IV compounds occupy the binding pocket and the tunnel, but do not contact the catalytic site. Such compounds have been discovered either by design, fusing parts of a type I and a type III inhibitor, such as in FP-Cpd-17 ( $IC_{50} = 14$  nM) [49], or by serendipity, during a high-throughput screen followed by specific structure-based design, such as in GLPG1690 [64] (Figure 8).

We reported the structure-guided design and chemical evolution of bile salts, from weak physiological non-competitive inhibitors into potent competitive type IV compounds [49]. This was achieved by using the PF-8380 dichlorocarbamate moiety as a pocket-binding lipophilic portion. By design, these compounds did not interact with the active site residues, but still hampered LPC or LPA binding. The best lead compounds differed chiefly regarding spacers connecting the steroid and the dichlorocarbamate moieties: linear amide linker, piperazine, or piperidine for FP-Cpd-5 ( $IC_{50} = 202$  nM; LPC), 11 ( $IC_{50} = 814$  nM; LPC) and 17 ( $IC_{50} = 20$  nM; LPC), respectively (Figure 8) [49]. Moreover, a very short spacer yielded no measurable inhibitory activity, which explains why FP-Cpd-11 exhibited a five-fold lower activity than FP-Cpd-17. These compounds were co-crystallized with rat ATX, showing how this type of inhibitors accommodate at both the tunnel and the pocket. Specifically, they all made Hydrogen bonds with Tyr81 and Trp260 at the tunnel and established  $\pi$ - $\pi$  interactions with Phe273 and Trp274 in the hydrophobic pocket (Figure 8, Table 1) [49]. Lastly,

these type IV compounds were used in *in vitro* cell assays, where they showed a decrease of LPA-driven downstream phosphorylation of Akt in BJeH fibroblasts [49].

The Belgo-Dutch company Galapagos NV serendipitously discovered the only other confirmed type IV compound series. They used a high throughput screen, where they identified an imidazo[1,2-a]pyridine series, from which the very potent compounds GLPG1690 ( $IC_{50} = 27$  nM; LPC) [64] and AJ-Cpd-9 ( $IC_{50} = 357$  nM; LPC) [39] were obtained by structure-activity evolution (Figure 8). Moreover, the crystal structures of these compounds confirmed their binding mode to ATX. GLPG1690 makes a Hydrogen bond with Trp254,  $\pi$ - $\pi$  interactions Phe274 and further hydrophobic interactions with Phe250 and Phe275. AJ-Cpd-9 makes a Hydrogen bond with Trp260 and hydrophobic interactions with Trp254, Phe250, Phe260 and Phe275 (Figure 8, Table 1). After pharmacokinetics and pharmacodynamics analyses [65,66], *in vivo* experiments showed that administration of GLPG1690 to bleomycin-treated mice resulted in a reduction of lung fibrosis, which was linked to a dose-dependent reduction of plasma LPA 18:2 levels (90%) (Table 2) [39,64]. This compound has shown very promising results in advanced clinical trials against idiopathic lung fibrosis and has recently progressed to phase III clinical trials for IPF [67].

## An Interplay between Inhibitor Types and Autotaxin Function?

The different types of ATX inhibitors could have different outcomes that go beyond the simple orthosteric inhibition of catalytic activity. While we know that LPA binding to the allosteric site is likely increasing the catalytic rate of ATX, possible roles of the tunnel in delivering LPA to receptors, perhaps in an interplay between surface integrins and proteoglycans, have not been exploited. The fact that Edg and non-Edg receptors have different binding pocket characteristics, could imply that LPA delivery through the tunnel, could be receptor-dependent.

Type I inhibitors would effectively stop LPA production from LPC, but would not affect any independent function of the allosteric site. Type IV inhibitors however, would also abolish any functionality of the allosteric site, expelling bound LPA. We suggest that the clinical success of the type IV compound GLPG1690 is not independent from its mode of binding and inhibition, interfering with the allosteric tunnel. Albeit ATX inhibitors were not successful in animal cancer models, at least to our knowledge, one should consider the different types of inhibitors in the context of cancer therapy. A type IV inhibitor, occupying the low-affinity allosteric tunnel could prove much more effective in the context of a tumour with high local LPA concentration that could displace the inhibitor from the high-affinity orthosteric site. It is our expectation that Autotaxin inhibitors will have a dynamic come back in the context of cancer therapy.

### Funding

Funding for ATX research has been provided by NWO-TOP (700.10.354) and by the Oncode Institute to AP.

### Conflict of Interests

The authors declare that have no conflicts of interest with the contents of this article.

### Acknowledgements

We would like to thank Wouter Moolenaar for critically reading the manuscript.

## References

1. van Corven, E.; Groenink, A.; Jalink, K.; Eichholtz, T.; Moolenaar, W. Lysophosphatidate-induced cell proliferation: identification and dissection of signaling pathways mediated by G proteins. *Cell* **1989**, *59*, 45–54.
2. Jalink, K.; Van Corven, E.J.; Moolenaar, W.H. Lysophosphatidic acid, but not phosphatidic acid, is a potent Ca<sup>2+</sup>-mobilizing stimulus for fibroblasts: Evidence for an extracellular site of action. *J. Biol. Chem.* **1990**, *265*, 12232–12239.
3. Wang, J.; Sun, Y.; Qu, J.; Yan, Y.; Yang, Y.; Cai, H. Roles of LPA receptor signaling in breast cancer. *Expert Rev. Mol. Diagn.* **2016**, *16*, 1103–1111.
4. Kaffe, E.; Katsifa, A.; Xylourgidis, N.; Ninou, I.; Zannikou, M.; Harokopos, V.; Foka, P.; Dimitriadis, A.; Evangelou, K.; Moulas, A.N.; et al. Hepatocyte autotaxin expression promotes liver fibrosis and cancer. *Hepatology* **2017**, *65*, 1369–1383.
5. Tager, A.M.; LaCamera, P.; Shea, B.S.; Campanella, G.S.; Selman, M.; Zhao, Z.; Polosukhin, V.; Wain, J.; Karimi-Shah, B.A.; Kim, N.D.; et al. The lysophosphatidic acid receptor LPA1 links pulmonary fibrosis to lung injury by mediating fibroblast recruitment and vascular leak. *Nat. Med.* **2008**, *14*, 45–54.
6. Kremer, A.E.; Martens, J.J.W.W.; Kulik, W.; Ruëff, F.; Kuiper, E.M.M.; van Buuren, H.R.; van Erpecum, K.J.; Kondrackiene, J.; Prieto, J.; Rust, C.; et al. Lysophosphatidic acid is a potential mediator of cholestatic pruritus. *Gastroenterology* **2010**, *139*, 1018.e1-1018.
7. Barbayiannia, E.; Kaffeb, E.; Aidinisb, V.; Kokotos, G. Autotaxin, a secreted lysophospholipase D, as a promising therapeutic target in chronic inflammation and cancer. *Prog. Lipid Res.* **2015**, *58*, 76–96.
8. Benesch, M.G.K.; Tang, X.; Venkatraman, G.; Bekele, R.T.; Brindley, D.N. Recent advances in targeting the autotaxin-lysophosphatidate-lipid phosphate phosphatase axis in vivo. *J. Biomed. Res.* **2016**, *30*, 272–284.
9. Chrencik, J.E.; Roth, C.B.; Terakado, M.; Kurata, H.; Omi, R.; Kihara, Y.; Warshaviak, D.; Nakade, S.; Asmar-Rovida, G.; Mileni, M.; et al. Crystal Structure of Antagonist Bound Human Lysophosphatidic Acid Receptor 1. *Cell* **2015**, *161*, 1633–1643.
10. Taniguchi, R.; Inoue, A.; Sayama, M.; Uwamizu, A.; Yamashita, K.; Hirata, K.; Yoshida, M.; Tanaka, Y.; Kato, H.E.; Nakada-Nakura, Y.; et al. Structural insights into ligand recognition by the lysophosphatidic acid receptor LPA6. *Nature* **2017**, *548*, 356–360.
11. Zhang, H.; Pluhackova, K.; Jiang, Z.; Böckmann, R.A. Binding Characteristics of Sphingosine-1-Phosphate to ApoM hints to Assisted Release Mechanism via the ApoM Calyx-Opening. *Sci. Rep.* **2016**, *6*, 30655.
12. Stanley, N.; Pardo, L.; Fabritiis, G. De The pathway of ligand entry from the membrane bilayer to a lipid G protein-coupled receptor. *Sci. Rep.* **2016**, *6*, 1–9.
13. Albers, H.M.H.G.; Dong, A.; van Meeteren, L.A.; Egan, D.A.; Sunkara, M.; van Tilburg, E.W.; Schuurman, K.; van Tellingen, O.; Morris, A.J.; Smyth, S.S.; et al. Boronic acid-based inhibitor of autotaxin reveals rapid turnover of LPA in the circulation. *Proc. Natl. Acad. Sci. U. S. A.* **2010**, *107*, 7257–7262.
14. Tomsig, J.L.; Snyder, A.H.; Berdyshev, E.V.; Skobeleva, A.; Mataya, C.; Natarajan, V.; Brindley, D.N.; Lynch, K.R. Lipid phosphate phosphohydrolase type 1 (LPP1) degrades extracellular lysophosphatidic

acid *in vivo*. *Biochem. J.* **2009**, *419*, 611–618.

15. Tang, X.; Benesch, M.G.K.; Dewald, J.; Zhao, Y.Y.; Patwardhan, N.; Santos, W.L.; Curtis, J.M.; McMullen, T.P.W.; Brindley, D.N. Lipid phosphate phosphatase-1 expression in cancer cells attenuates tumor growth and metastasis in mice. *J. Lipid Res.* **2014**, *55*, 2389–2400.
16. Jasinska, R.; Zhang, Q.; Pilquill, C.; Singh, I.; Xu, J.; Dewald, J.; Dillon, D.A.; Berthiaume, L.G.; Carman, G.M.; Waggoner, D.W.; et al. Lipid phosphate phosphohydrolase-1 degrades exogenous glycerolipid and sphingolipid phosphate esters. **1999**, *340*, 677–686.
17. van Meeteren, L.A.; Moolenaar, W.H. Regulation and biological activities of the autotaxin-LPA axis. *Prog. Lipid Res.* **2007**, *46*, 145–160.
18. Aoki, J.; Taira, A.; Takanezawa, Y.; Kishi, Y.; Hama, K.; Kishimoto, T.; Mizuno, K.; Saku, K.; Taguchi, R.; Arai, H. Serum lysophosphatidic acid is produced through diverse phospholipase pathways. *J. Biol. Chem.* **2002**, *277*, 48737–48744.
19. Umezu-Goto, M.; Kishi, Y.; Taira, A.; Hama, K.; Dohmae, N.; Takio, K.; Yamori, T.; Mills, G.B.; Inoue, K.; Aoki, J.; et al. Autotaxin has lysophospholipase D activity leading to tumor cell growth and motility by lysophosphatidic acid production. *J. Cell Biol.* **2002**, *158*, 227–233.
20. Matralis, A.N.; Afantitis, A.; Aidinis, V. Development and therapeutic potential of autotaxin small molecule inhibitors: From bench to advanced clinical trials. *Med. Res. Rev.* **2019**, *39*, 976–1013.
21. Tokumura, A.; Majima, E.; Kariya, Y.; Tominaga, K.; Kogure, K.; Yasuda, K.; Fukuzawa, K. Identification of human plasma lysophospholipase D, a lysophosphatidic acid-producing enzyme, as autotaxin, a multifunctional phosphodiesterase. *J. Biol. Chem.* **2002**, *277*, 39436–39442.
22. Jansen, S. Proteolytic maturation and activation of autotaxin (NPP2), a secreted metastasis-enhancing lysophospholipase D. *J. Cell Sci.* **2005**, *118*, 3081–3089.
23. Hausmann, J.; Keune, W.-J.; Hipgrave Ederveen, A.L.; van Zeijl, L.; Joosten, R.P.; Perrakis, A. Structural snapshots of the catalytic cycle of the phosphodiesterase Autotaxin. *J. Struct. Biol.* **2016**, *195*, 199–206.
24. Hausmann, J.; Kamtekar, S.; Christodoulou, E.; Day, J.E.; Wu, T.; Fulkerson, Z.; Albers, H.M.H.G.H.G.; Van Meeteren, L.A.; Houben, A.J.S.S.; Van Zeijl, L.; et al. Structural basis for substrate discrimination and integrin binding by autotaxin. *Nat. Struct. Mol. Biol.* **2011**, *18*, 198–204.
25. Keune, W.; Hausmann, J.; Bolier, R.; Tolenaars, D.; Kremer, A.; Heidebrecht, T.; Joosten, R.; Sunkara, M.; Morris, A.; Matas-Rico, E.; et al. Steroid binding to Autotaxin links bile salts and lysophosphatidic acid signalling. *Nat. Commun.* **2016**, *7*, 11248.
26. Nishimasu, H.; Okudaira, S.; Hama, K.; Mihara, E.; Dohmae, N.; Inoue, A.; Ishitani, R.; Takagi, J.; Aoki, J.; Nureki, O. Crystal structure of autotaxin and insight into GPCR activation by lipid mediators. *Nat. Struct. Mol. Biol.* **2011**, *18*, 205–212.
27. Salgado-Polo, F.; Fish, A.; Matsoukas, M.-T.; Heidebrecht, T.; Keune, W.-J.; Perrakis, A. Lysophosphatidic acid produced by Autotaxin acts as an allosteric modulator of its catalytic efficiency. *J. Biol. Chem.* **2018**, *293*, jbc.RA118.004450.
28. Saunders, L.P.; Cao, W.; Chang, W.C.; Albright, R. a; Braddock, D.T.; De La Cruz, E.M. Kinetic analysis of autotaxin reveals substrate-specific catalytic pathways and a mechanism for lysophosphatidic acid distribution. *J. Biol. Chem.* **2011**, *286*, 30130–41.

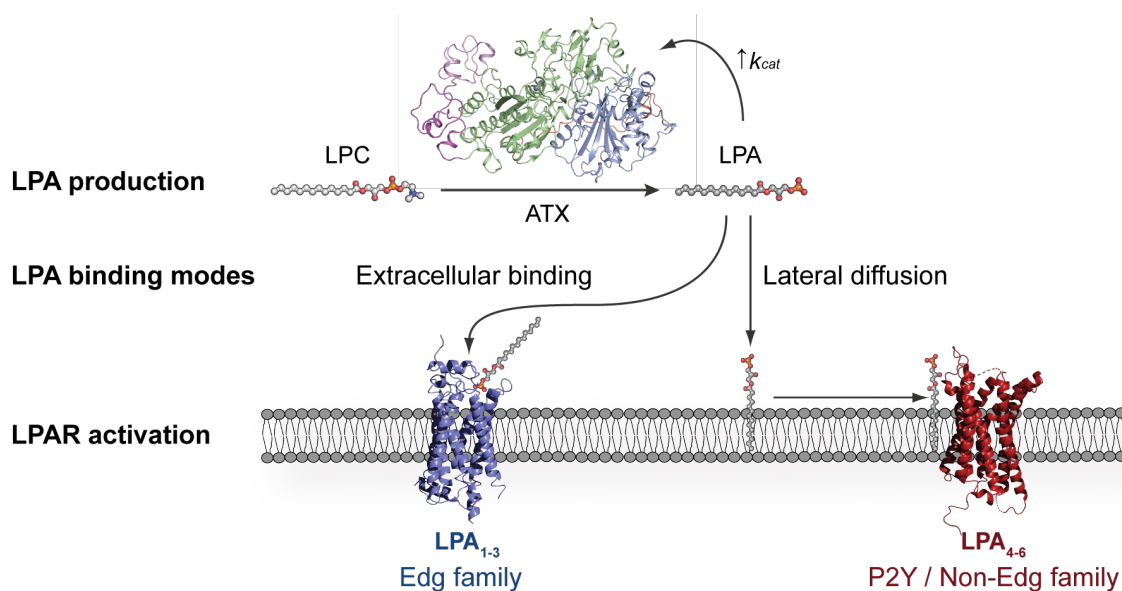
29. Jethwa, S.A.; Leah, E.J.; Zhang, Q.; Bright, N.A.; Oxley, D.; Bootman, M.D.; Rudge, S.A.; Wakelam, M.J.O. Exosomes bind to autotaxin and act as a physiological delivery mechanism to stimulate LPA receptor signalling in cells. *J. Cell Sci.* **2016**, *129*, 3948–3957.
30. Leblanc, R.; Lee, S.C.; David, M.; Bordet, J.C.; Norman, D.D.; Patil, R.; Miller, D.; Sahay, D.; Ribeiro, J.; Clezardin, P.; et al. Interaction of platelet-derived autotaxin with tumor integrin alphaVbeta3 controls metastasis of breast cancer cells to bone. *Blood* **2014**, *124*, 3141–3150.
31. Wu, T.; Kooi, C. Vander; Shah, P.; Charnigo, R.; Huang, C.; Smyth, S.S.; Morris, A.J. Integrin-mediated cell surface recruitment of autotaxin promotes persistent directional cell migration. *FASEB J.* **2014**, *28*, 861–870.
32. Fulkerson, Z.; Wu, T.; Sunkara, M.; Kooi, C. Vander; Morris, A.J.; Smyth, S.S. Binding of autotaxin to integrins localizes lysophosphatidic acid production to platelets and mammalian cells. *J. Biol. Chem.* **2011**, *286*, 34654–34663.
33. Pamuklar, Z.; Federico, L.; Liu, S.; Umezu-Goto, M.; Dong, A.; Panchatcharam, M.; Fulerson, Z.; Berdyshev, E.; Natarajan, V.; Fang, X.; et al. Autotaxin/Lysopholipase D and lysophosphatidic acid regulate murine hemostasis and thrombosis. *J. Biol. Chem.* **2009**, *284*, 7385–7394.
34. Houben, A.J.S.; Van Wijk, X.M.R.; Van Meeteren, L.A.; Van Zeijl, L.; Van De Westerlo, E.M.A.; Hausmann, J.; Fish, A.; Perrakis, A.; Van Kuppevelt, T.H.; Moolenaar, W.H. The polybasic insertion in autotaxin ?? confers specific binding to heparin and cell surface heparan sulfate proteoglycans. *J. Biol. Chem.* **2013**, *288*, 510–519.
35. Castagna, D.; Budd, D.C.; Macdonald, S.J.F.F.; Jamieson, C.; Watson, A.J.B.B. Development of Autotaxin Inhibitors: An Overview of the Patent and Primary Literature. *J. Med. Chem.* **2016**, *59*, 5604–5621.
36. Nikolaou, A.; Kokotou, M.G.; Limnios, D.; Psarra, A.; Kokotos, G. Autotaxin inhibitors: a patent review (2012-2016). *Expert Opin. Ther. Pat.* **2017**, *27*, 815–829.
37. Lynch, K.R.; Macdonald, T.L. Phosphonate derivatives as Autotaxin inhibitors 2013.
38. Kato, K.; Ikeda, H.; Miyakawa, S.; Futakawa, S.; Nonaka, Y.; Fujiwara, M.; Okudaira, S.; Kano, K.; Aoki, J.; Morita, J.; et al. Structural basis for specific inhibition of Autotaxin by a DNA aptamer. *Nat. Struct. Mol. Biol.* **2016**, *23*, 395–401.
39. Joncour, A.; Desroy, N.; Housseman, C.; Bock, X.; Bienvenu, N.; Cherel, L.; Labeguere, V.; Peixoto, C.; Annot, D.; Lepissier, L.; et al. Supporting information Discovery , Structure-Activity Relationship and Binding Mode of an Imidazo [ 1 , 2- a ] pyridine Series of Autotaxin Inhibitors. 1–15.
40. Baker, L.D.; Fujiwara, Y.; Pigg, K.; Tsukahara, R.; Kobatashi, S.; Murofushi, H.; Uchiyama, A.; Murakami-Murofushi, K.; Murph, E.; Mills, G.B.; et al. Carba analogs of cyclic phosphatidic acid are selective inhibitors of autotaxin and cancer cell invasion and metastasis. *J Biol Chem* **2006**, *281*, 22786–22793.
41. Durgam, G.G.; Virag, T.; Walker, M.D.; Tsukahara, R.; Yasuda, S.; Liliom, K.; van Meeteren, L.A.; Moolenaar, W.H.; Wilke, N.; Siess, W.; et al. Synthesis, Structure–Activity Relationships, and Biological Evaluation of Fatty Alcohol Phosphates as Lysophosphatidic Acid Receptor Ligands, Activators of PPAR $\gamma$ , and Inhibitors of Autotaxin. *J. Med. Chem.* **2005**, *48*, 4919–4930.
42. Nikitopoulou, I.; Kaffe, E.; Sevastou, I.; Sirioti, I.; Samiotaki, M.; Madan, D.; Prestwich, G.D.; Aidinis, V. A Metabolically-Stabilized Phosphonate Analog of Lysophosphatidic Acid Attenuates Collagen-Induced Arthritis. *PLoS One* **2013**, *8*.

43. van Meeteren, L.A.; Brinkmann, V.; Saulnier-Blache, J.S.; Lynch, K.R.; Moolenaar, W.H. Anticancer activity of FTY720: Phosphorylated FTY720 inhibits autotaxin, a metastasis-enhancing and angiogenic lysophospholipase D. *Cancer Lett.* **2008**, *266*, 203–208.
44. Ferry, G.; Moulharat, N.; Pradere, J.-P.; Desos, P.; Try, A.; Genton, A.; Giganti, A.; Beucher-Gaudin, M.; Lonchamp, M.; Bertrand, M.; et al. S32826, A Nanomolar Inhibitor of Autotaxin: Discovery, Synthesis and Applications as a Pharmacological Tool. *J. Pharmacol. Exp. Ther.* **2008**, *327*, 809–819.
45. Albers, H.M.H.G.; Hendrickx, L.J.D.; van Tol, R.J.P.; Hausmann, J.; Perrakis, A.; Ovaa, H. Structure-based design of novel boronic acid-based inhibitors of autotaxin. *J. Med. Chem.* **2011**, *54*, 4619–4626.
46. Kawaguchi, M.; Okabe, T.; Okudaira, S.; Nishimasu, H.; Ishitani, R.; Kojima, H.; Nureki, O.; Aoki, J.; Nagano, T. Screening and X-ray crystal structure-based optimization of autotaxin (ENPP2) inhibitors, using a newly developed fluorescence probe. *ACS Chem. Biol.* **2013**, *8*, 1713–1721.
47. Jones, S.B.; Pfeifer, L.A.; Bleisch, T.J.; Beauchamp, T.J.; Durbin, J.D.; Klimkowski, V.J.; Hughes, N.E.; Rito, C.J.; Dao, Y.; Gruber, J.M.; et al. Novel Autotaxin Inhibitors for the Treatment of Osteoarthritis Pain: Lead Optimization via Structure-Based Drug Design. *ACS Med. Chem. Lett.* **2016**, *7*, 857–861.
48. Gierse, J.; Thorarensen, A.; Beltey, K.; Bradshaw-pierce, E.; Cortes-burgos, L.; Hall, T.; Johnston, A.; Murphy, M.; Nemirovskiy, O.; Ogawa, S.; et al. A Novel Autotaxin Inhibitor Reduced LysoPhosphatidic Acid Levels in Plasma and the Site of Inflammation. *J. Pharmacol. Exp. Ther.* **2010**, *2*, 310–317.
49. Keune, W.J.; Potjewyd, F.; Heidebrecht, T.; Salgado-Polo, F.; Macdonald, S.J.F.; Chelvarajan, L.; Abdel Latif, A.; Soman, S.; Morris, A.J.; Watson, A.J.B.; et al. Rational Design of Autotaxin Inhibitors by Structural Evolution of Endogenous Modulators. *J. Med. Chem.* **2017**, *60*, 2006–2017.
50. Katsifa, A.; Kaffe, E.; Nikolaidou-Katsaridou, N.; Economides, A.N.; Newbigging, S.; McKerlie, C.; Aidinis, V. The bulk of autotaxin activity is dispensable for adult mouse life. *PLoS One* **2015**, *10*, 1–14.
51. Ninou, I.; Kaffe, E.; Müller, S.; Budd, D.C.; Stevenson, C.S.; Ullmer, C.; Aidinis, V. Pharmacologic targeting of the ATX/LPA axis attenuates bleomycin-induced pulmonary fibrosis. *Pulm. Pharmacol. Ther.* **2018**, *52*, 32–40.
52. Weng, J.; Jiang, S.; Ding, L.; Xu, Y.; Zhu, X.; Jin, P. Autotaxin/lysophosphatidic acid signaling mediates obesity-related cardiomyopathy in mice and human subjects. *J. Cell. Mol. Med.* **2019**, *23*, 1050–1058.
53. Kuttruff, C.A.; Ferrara, M.; Bretschneider, T.; Hoerer, S.; Handschuh, S.; Nosse, B.; Romig, H.; Nicklin, P.; Roth, G.J. Discovery of BI-2545: A Novel Autotaxin Inhibitor That Significantly Reduces LPA Levels in Vivo. *ACS Med. Chem. Lett.* **2017**, *8*, 1252–1257.
54. Stein, A.J.; Bain, G.; Prodanovich, P.; Santini, A.M.; Darlington, J.; Stelzer, N.M.P.; Sidhu, R.S.; Schaub, J.; Goulet, L.; Lonergan, D.; et al. Structural Basis for Inhibition of Human Autotaxin by Four Potent Compounds with Distinct Modes of Binding. *Mol. Pharmacol.* **2015**, *88*, 982–992.
55. Shah, P.; Cheasty, A.; Foxton, C.; Raynham, T.; Farooq, M.; Gutierrez, I.F.; Lejeune, A.; Pritchard, M.; Turnbull, A.; Pang, L.; et al. Discovery of potent inhibitors of the lysophospholipase autotaxin. *Bioorganic Med. Chem. Lett.* **2016**, *26*, 5403–5410.
56. Jiang, G.; Madan, D.; Prestwich, D., G. Aromatic Phosphonates Inhibit the Lydophosphodiesterase D Activity of Autotaxin. **2011**, *21*, 5098–5101.
57. Bain, G.; Shannon, K.E.; Huang, F.; Darlington, J.; Goulet, L.; Prodanovich, P.; Ma, G.L.; Santini, A.M.; Stein, A.J.; Lonergan, D.; et al. Selective Inhibition of Autotaxin Is Efficacious in Mouse Models of

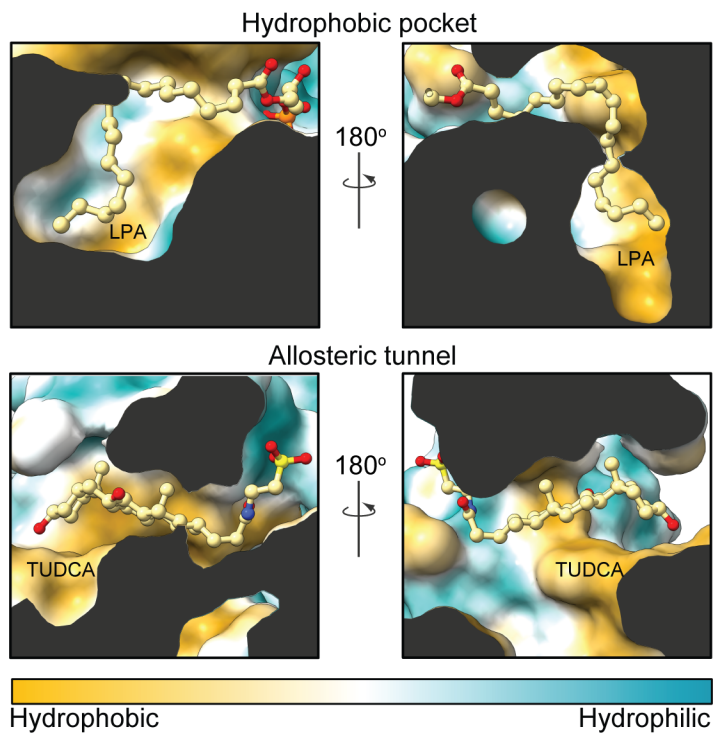
Liver Fibrosis s. **2017**, *2*.

58. Black, K.E.; Berdyshev, E.; Bain, G.; Castellino, F. V.; Shea, B.S.; Probst, C.K.; Fontaine, B.A.; Bronova, I.; Goulet, L.; Lagares, D.; et al. Autotaxin activity increases locally following lung injury, but is not required for pulmonary lysophosphatidic acid production or fibrosis. *FASEB J.* **2016**.
59. Castellino, F. V.; Bain, G.; Pace, V.A.; Black, K.E.; George, L.; Probst, C.K.; Goulet, L.; Lafyatis, R.; Tager, A.M. HHS Public Access. **2016**, *68*, 2964–2974.
60. Roppe, J.R.; Parr, T.A.; Stock, N.S.; Volkots, D.; Hutchinson, J.H. Autotaxin inhibitors and uses thereof 2012.
61. Evans, J.F. Methods and compositions for the treatment of metabolic disorders 2016.
62. Hutchinson, J.H.; Parr, T.A.; Roppe, J.R.; Stock, N.S.; Volkots, D. Heterocyclic autotaxin inhibitors and uses thereof 2012.
63. Miller, L.M.; Keune, W.J.; Castagna, D.; Young, L.C.; Duffy, E.L.; Potjewyd, F.; Salgado-Polo, F.; García, P.E.; Semaan, D.; Pritchard, J.M.; et al. Structure-activity relationships of small molecule autotaxin inhibitors with a discrete binding mode. *J. Med. Chem.* **2017**, *60*, 722–748.
64. Desroy, N.; Housseman, C.; Bock, X.; Joncour, A.; Bienvenu, N.; Cherel, L.; Labeguere, V.; Rondet, E.; Peixoto, C.; Grassot, J.-M.; et al. Discovery of 2-[[2-Ethyl-6-[4-[2-(3-hydroxyazetidin-1-yl)-2-oxoethyl]piperazin-1-yl]-8-methylimidazo[1,2-*a*]pyridin-3-yl]methylamino]-4-(4-fluorophenyl)thiazole-5-carbonitrile (GLPG1690), a First-in-Class Autotaxin Inhibitor Undergoing Clinical Ev. *J. Med. Chem.* **2017**.
65. Blanque, R. D. N.; Dupont, S.; Cottreaux, C.; Marsais, F.; Lepescheux, L.; Monjardet, A.; Wakselman, E.; Laenen, W.; Russell, V.; van der Aar, E.; Brys, R.; Heckmann, B. Pharmacological profile and efficacy of GLPG1690, a novel ATX inhibitor for COPD treatment Available online: [http://files.glp.com/docs/website\\_1/Poster\\_ERS\\_2015\\_final.pdf](http://files.glp.com/docs/website_1/Poster_ERS_2015_final.pdf).
66. Maher, T.M.; van der Aar, E.M.; Van de Steen, O.; Allamassey, L.; Desrivot, J.; Dupont, S.; Fagard, L.; Ford, P.; Fieuw, A.; Wuyts, W. Safety, tolerability, pharmacokinetics, and pharmacodynamics of GLPG1690, a novel autotaxin inhibitor, to treat idiopathic pulmonary fibrosis (FLORA): a phase 2a randomised placebo-controlled trial. *Lancet Respir. Med.* **2018**, *6*, 627–635.
67. Galapagos announces ISABELA Phase 3 program in IPF Available online: <http://hugin.info/133350/R/2183965/843660.pdf>.
68. Ninou, I.; Magkrioti, C.; Aidinis, V. Autotaxin in Pathophysiology and Pulmonary Fibrosis. *Front. Med.* **2018**, *5*, 1–11.
69. Bhave, S.R.; Dadey, D.Y.A.; Karvas, R.M.; Ferraro, D.J.; Kotipatruni, R.P.; Jaboin, J.J.; Hallahan, A.N.; DeWees, T.A.; Linkous, A.G.; Hallahan, D.E.; et al. Autotaxin Inhibition with PF-8380 Enhances the Radiosensitivity of Human and Murine Glioblastoma Cell Lines. *Front. Oncol.* **2013**, *3*, 1–11.
70. Nikolaou, A.; Ninou, I.; Kokotou, M.G.; Kaffe, E.; Afantitis, A.; Aidinis, V.; Kokotos, G. Hydroxamic Acids Constitute a Novel Class of Autotaxin Inhibitors that Exhibit in Vivo Efficacy in a Pulmonary Fibrosis Model. *J. Med. Chem.* **2018**, *61*, 3697–3711.
71. Lee, S.; Fujiwara, Y.; Liu, J.; Yue, J.; Shimizu, Y.; Norman, D.; Wang, Y.; Tsukahara, R.; Szabo, E.; Patil, R.; et al. Autotaxin, LPA Receptors (1 and 5) Exert Disparate Functions in Tumor Cells Versus the Host Tissue Microenvironment in Melanoma Invasion and Metastasis. *Mol Cancer Res* **2015**, *13*, 174–185.

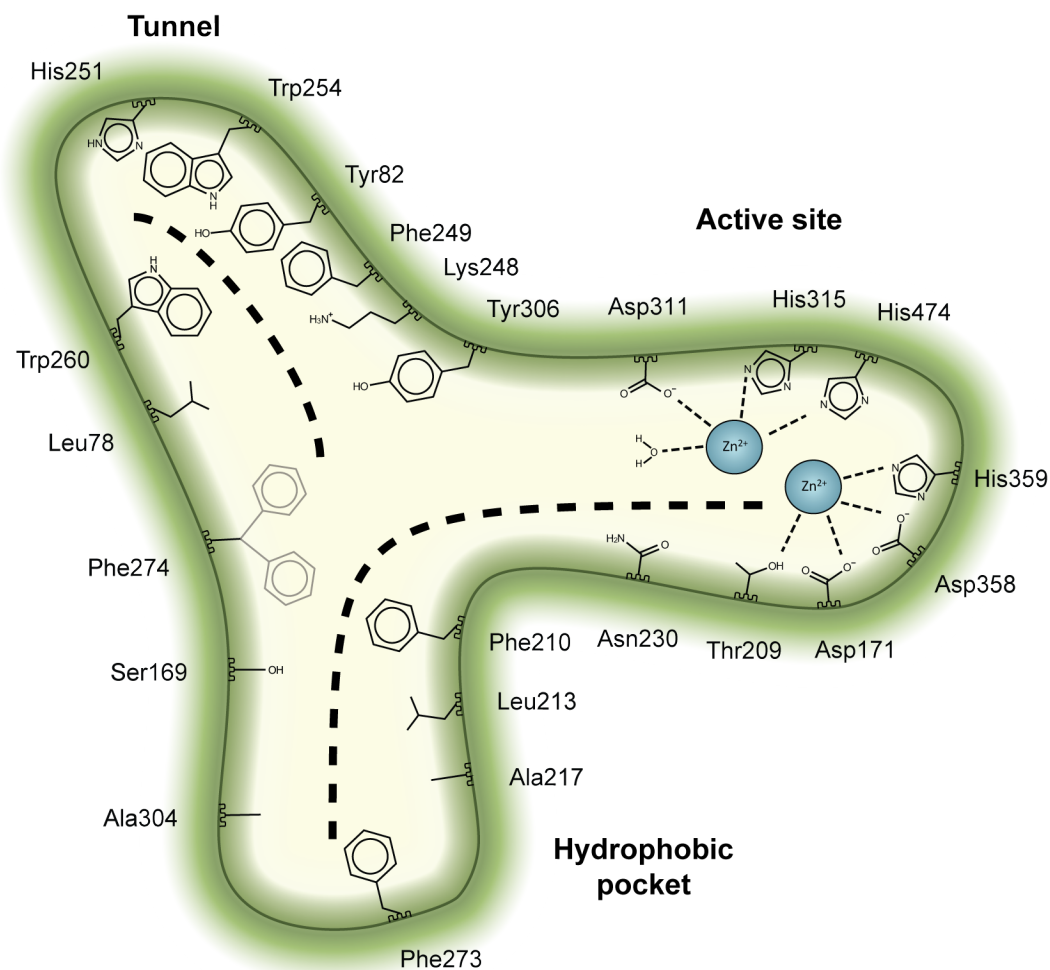
72. Oikonomou, N.; Mouratis, M.A.; Tzouveleakis, A.; Kaffe, E.; Valavanis, C.; Vilaras, G.; Karameris, A.; Prestwich, G.D.; Bouros, D.; Aidinis, V. Pulmonary autotaxin expression contributes to the pathogenesis of pulmonary fibrosis. *Am. J. Respir. Cell Mol. Biol.* **2012**, *47*, 566–574.
73. Park, G.Y.; Lee, Y.G.; Berdyshev, E.; Nyenhuis, S.; Du, J.; Fu, P.; Gorshkova, I.A.; Li, Y.; Chung, S.; Karpurapu, M.; et al. Autotaxin production of lysophosphatidic acid mediates allergic asthmatic inflammation. *Am. J. Respir. Crit. Care Med.* **2013**, *188*, 928–940.
74. Study to Assess Safety, Tolerability, Pharmacokinetic and Pharmacodynamic Properties of GLPG1690. Available online: <https://clinicaltrials.gov/ct2/show/NCT02738801>.
75. Benesch, M.G.K.; Tang, X.; Maeda, T.; Ohhata, A.; Zhao, Y.Y.; Kok, B.P.C.; Dewald, J.; Hitt, M.; Curtis, J.M.; McMullen, T.P.W.; et al. Inhibition of autotaxin delays breast tumor growth and lung metastasis in mice. *FASEB J.* **2014**, *28*, 2655–2666.
76. Benesch, M.G.K.; Zhao, Y.Y.; Curtis, J.M.; McMullen, T.P.W.; Brindley, D.N. Regulation of autotaxin expression and secretion by lysophosphatidate and sphingosine 1-phosphate. *J. Lipid Res.* **2015**, *56*, 1134–1144.



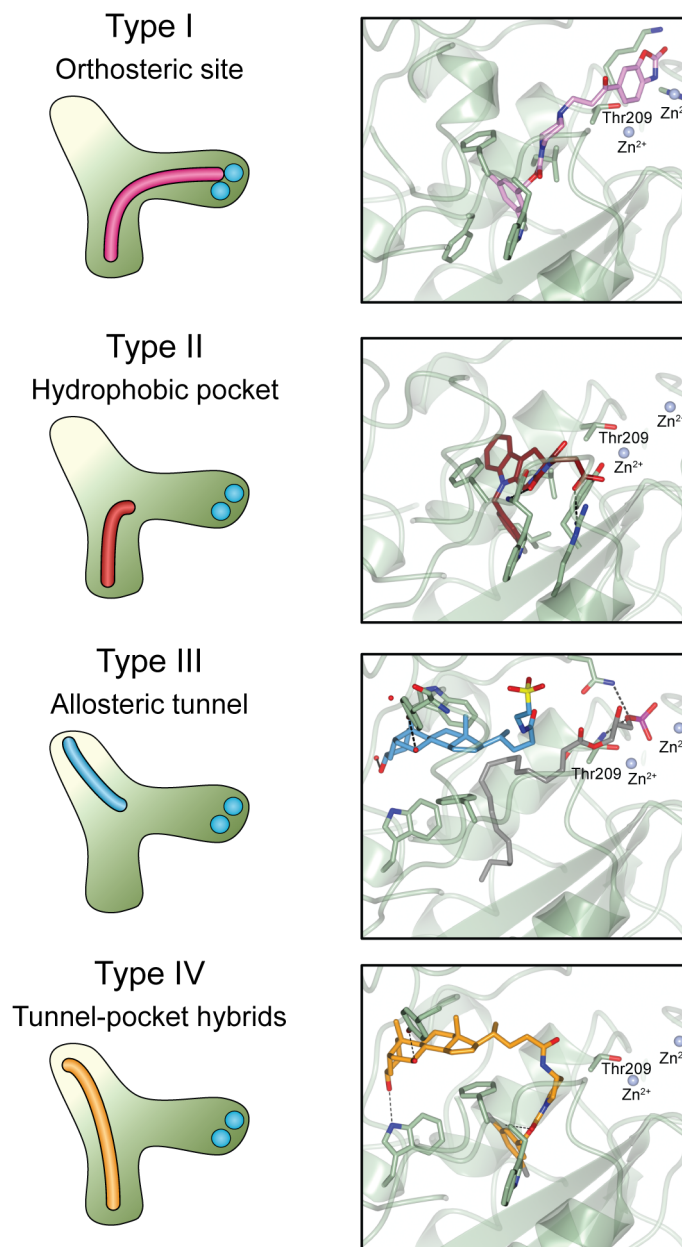
**Figure 1. Distinct modes for LPA binding to its cognate GPCRs proposed based on their crystallographic structures.** ATX is the main producer of LPA, which can then bind to the extracellularly open lipid-binding pocket of LPA<sub>1-3</sub>, potentially assisted by lipid chaperones, or diffuse laterally towards the membrane-open ligand-binding site of LPA<sub>4-6</sub>.



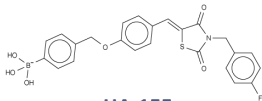
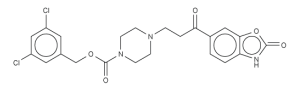
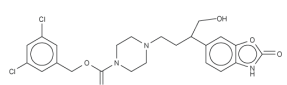
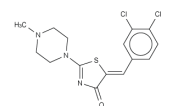
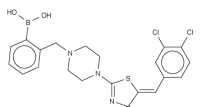
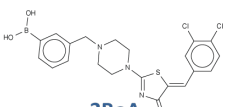
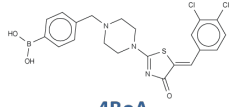
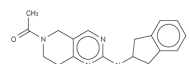
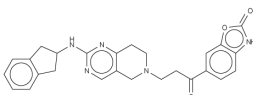
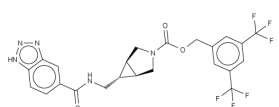
**Figure 2. Hydrophobicity comparison between the hydrophobic pocket and the allosteric tunnel.** Side sections of ATX (PDB: 5dlw) showing the modes of binding of LPA and TUDCA in the orthosteric and allosteric sites, respectively. The narrow partly hydrophobic tunnel presents hydrophilic patches that accommodate the polar moieties of TUDCA. Protein surface was coloured from orange to turquoise using ChimeraX (version 0.91).



**Figure 3.** Key residues involved in binding the four classes of ATX inhibitors. **A**, Cartoon depiction of the ATX tripartite site and the crucial interacting residues for inhibitor binding. The dashed lines depict the binding site for type LPC or LPA at the orthosteric site, as well as the binding site for steroids at the tunnel.



**Figure 4.** Classification of the four reported ATX inhibitor types based on their binding modes. **Left**, schematic view of the binding modes. **Right**, crystallographic structures of ATX bound to compounds from each type. From top to bottom: PF-8380 (5l0k), PAT-352 (4zg9), TUDCA (5dlw) and FP-Cpd 17 (5m0m).

 Type I Inhibitor	PDB ID	Activity (IC <sub>50</sub> )	References
 <b>HA-155</b>	2xrg	5.7 nM	[24,46]
 <b>PF-8380</b>	5l0k	1.7 nM	[48,49]
 <b>FP-Cpd 3</b>	5m0e	-	[50]
 <b>MK-Cpd 10</b>	3wav	180 nM*	[47]
 <b>2BoA</b>	3waw	580 nM*	[47]
 <b>3BoA</b>	3wax	13 nM*	[47]
 <b>4BoA</b>	3way	22 nM*	[47]
 <b>SBJ-Cpd 1</b>	5l0b	520 nM	[47]
 <b>SBJ-Cpd 2</b>	5l0e	2.5 nM	[48]
 <b>BI-2545</b>	5ohi	2.2 nM	[54]

\* TG-mTMP used as substrate

**Figure 5.** Type I ATX inhibitors based on their kinetic and crystallographic analysis.



## Type II Inhibitor

PDB ID

Activity (IC<sub>50</sub>)

References

<p><b>PAT-078</b></p>	4zg6	472 nM	[55]
<p><b>PAT-494</b></p>	4zga	20 nM	[55]
<p><b>PAT-352</b></p>	4zg9	26 nM	[55]
<p><b>CRT0273750</b></p>	5lia	1 nM	[56]

\*  $K_i$  value for FS-3 cleavage reported instead

**Figure 6.** Type II ATX inhibitors based on their kinetic and crystallographic analysis.

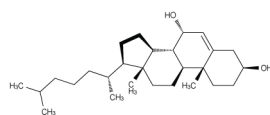


## Type III Inhibitor

PDB ID

Activity (IC<sub>50</sub>)

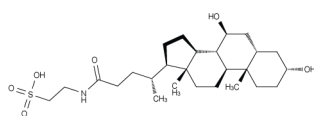
References

**7-α-hydroxycholesterol**

5dlt

undetermined

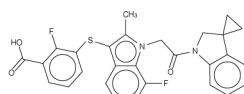
[25]

**TUDCA**

5dlw

10.4 μM

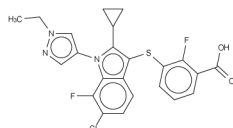
[25]

**PAT-347**

4zg7

0.3 nM

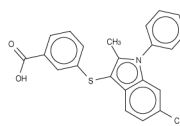
[55]

**PAT-505**

5kxa

2 nM

[58]

**LM-Cpd 51**

5lqq

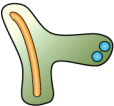
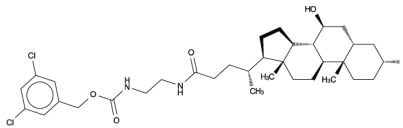
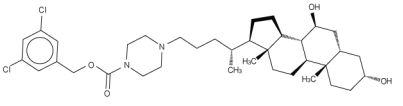
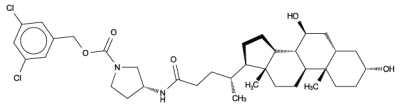
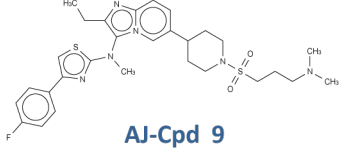
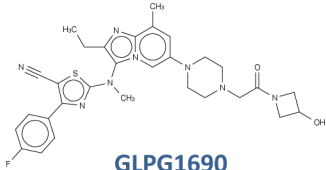
81 nM

[64]

\*\* based on structural similarities with PAT-505

\*\*\* structure of PharmAkea compound B is the same as PAT-505.

**Figure 7. Type III ATX inhibitors based on their kinetic and crystallographic analysis.**

 Type IV Inhibitor	PDB ID	Activity (IC <sub>50</sub> )	References
 <b>FP-Cpd 5</b>	5m0s	202 nM	[50]
 <b>FP-Cpd 11</b>	5m0d	814 nM	[50]
 <b>FP-Cpd 17</b>	5m0m	20 nM	[50]
 <b>AJ-Cpd 9</b>	5m7m	357 nM	[40]
 <b>GLPG1690</b>	5mhp	27 nM	[65]

**Figure 8.** Type IV ATX inhibitors based on their kinetic and crystallographic analysis.

**Table 1. Common interactions needed in distinct types of ATX inhibitors.**

Type	Residues establishing ligand contacts (rat ATX)		
	Active site – Hydrophilic groove	Hydrophobic pocket	Allosteric tunnel
I	Common	Thr209, Asp311, His474	-
	Frequent	His315, His359	Leu213, Phe273, Phe274*, Trp275
II	Common	-	Leu213, Phe274*, Trp276
	Frequent	-	Phe273, Tyr306
III	Common	-	Lys248, Phe249, Trp254, Trp260
	Frequent	-	Phe274*
IV	Common	-	Leu213, Phe273, Trp275, Tyr306
	Frequent	-	Phe274*, Phe210

\* Phe274 sidechain has two predominant conformers at the pocket-tunnel boundary depending on the interacting ligand.

**Table 2. ATX inhibitors employed in in vivo models. Further details discussed in [20,51,68].**

Type	Inhibitor	Disease	LPA inhibition	References
I	SBJ- Cpd 1	Inflammation Multiple sclerosis	>50%	[47]
I	PF-8380	Glioblastoma Liver fibrosis	>90% >90%	[69] [4]
I	GK442	Pulmonary fibrosis		[70]
I	BMP22	Melanoma metastasis	50%	[71]
II	GWJ-A-23	Pulmonary fibrosis inflammation	50%	[72] [73]
III	PharmAkea - Cpd A-E	Metabolic disorder	25-35%	[61]
III	PAT-505, PAT-048	Liver fibrosis Skin fibrosis	40-80%	[54]
IV	GLPG1690	Pulmonary fibrosis Clinical trials in IPF patients	84-95% 84-95%	[64] [74]
?	ONO-8430506	Breast cancer Thyroid cancer	>60% >70%	[75] [76]